Hindawi
Mathematical Problems in Engineering
Volume 2024, Article ID 7118127, 9 pages
https://doi.org/10.1155/2024/7118127

Research Article

One-Degree Aerial Device: Control and Experimental Development

Leonardo Acho,[1] **Pablo Buenestado**,[2] **and Gisela Pujol-Vázquez**[1]

[1]*Department of Mathematics, School of Industrial, Aerospace and Audiovisual Engineering of Terrassa (ESEIAAT), Universitat Polecnica de Catalunya, Terrassa, Spain*
[2]*Department of Mathematics, Barcelona East School of Engineering (EEBE), Universitat Polecnica de Catalunya, Barcelona, Spain*

Correspondence should be addressed to Leonardo Acho; leonardo.acho@upc.edu

Received 13 November 2023; Revised 24 January 2024; Accepted 29 January 2024; Published 10 February 2024

Academic Editor: Javier Moreno-Valenzuela

The ball and beam experimental platform is an unstable nonlinear system widely used as a benchmark control setup for testing different controller approaches, especially for beginners on automatic control to improve their control knowledge skills. In this paper, we innovate it by governing the angular position of the beam with a twin-rotor system. Our experiment consists of a beam that rotates through a pivot, in which two propellers are attached to the ends of this beam. Hence, we have a recent one-degree aerial device, and instead of using a ball, we employ a mass moving on the beam, presenting friction on position to its movements on the beam. Then, the control objective is to regulate the mass position at some predefined zone on the beam, ensuring stability and robustness in front of external perturbations and unmodeled uncertainties. To do so, we define a classical PI controller. To assess closed-loop robustness, a mass was introduced to one propeller to induce perturbation, thereby simulating modeling variations or disturbances. The experimental results prove the goodness of our experimental platform for drone applications.

1. Introduction

This paper introduces a new device to emulate the well-known ball and beam problem to a one-degree aerial device with a mass on the beam. Evidently, this device also presents high nonlinearities in its dynamics, which results in an important fact for an experimental benchmark to test control algorithms [1–3]. The performance of the obtained platform was tested by using a classical PI controller. Besides, the main objective to use a moving mass on the beam is to introduce a time-varying unbalanced center mass of gravity of the mechanism. Moreover, our designed platform is easy to construct at a low cost. Several experimental platforms using the ball and beam scheme have been reported in the past. For instance, in [4], a ball and beam system is constructed, and LabVIEW is employed for control and data management. Obviously, LabVIEW is not cheap software, and it requires some computational skills to drive it. Additionally, the used data acquisition card is also a technological challenger to set it in this application in coordination with LabVIEW. Saad and Khalallah [5] constructed a low-cost ball and beam system by using an Arduino-Uno electronic board for reading data and to supply the produced control signal. Also, they proved the efficacy of just using a PID controller to stabilize the system. Another low-cost ball and beam system is granted in [6], but it employs MATLAB and Simulink software for its operation. However, they still use a PID controller to stabilize their closed-loop system, and the one reported in [7] also has results that are interesting to read, among others [8]. In dealing with nonlinear systems, the widely recognized control algorithm is sliding mode control (SMC), which has been extensively utilized in various applications, including the ball-and-beam balancer [9]. However, a significant challenge associated with SMC is the occurrence of chattering, leading to potential noise amplification. The classic ball-and-beam system has served as a testing ground for more advanced control techniques, such as the data-driven design discussed in [10]. Nonetheless, our approach differs notably by incorporating an aerial device to balance the ball and introducing innovative design and modeling methodologies.

On the other hand, small unmanned aerial vehicles have been used in many applications, such as search and rescue,

remote inspection, and aerial videography [11]. In [12], the authors used a one-degree-aerial device to show the effectiveness of a novel sliding-mode control algorithm. According to them, this aerial mechanism can emulate the behavior of vertical-take-off planes. Even when this device has two propellers to manipulate a pivoted beam, just one of them is actuated under the control algorithm, and the other one is supplied with a fixed command signal. Experimentally, their control performance presents a variability of the behavior of the closed-loop system but shows stability. It is important to highlight that the use of pulse-width modulation (PWM) from the control signal to a DC motor of the propeller is almost mandatory for the speed control of a DC motor [13, 14]. Finally, Chai et al.[15] provide an overview of advanced guidance and control methods on aerial devices, analyzing various AI techniques.

This paper offers several key contributions:

(1) The development of a low-cost experimental platform of a one-degree-aerial device. It allows for hands-on experimentation, analysis, and validation of theoretical concepts in a real-world setting without the complexities or high costs associated with advanced aerial systems.
(2) A designed experimental platform for testing control algorithms featuring the inclusion of a breadboard. The aim is to build a functional prototype that enables experimentation and testing of various control methodologies for aerial stability.
(3) A novel design on electronic circuits. To the best of the authors' knowledge, there are no existing references or prior works on this specific design. Furthermore, detailed circuit schematics are provided to facilitate replication and understanding.
(4) A robustness study was conducted by introducing an additional mass to the propeller during the experiment. This modification allowed for simulations that account for unmodeled uncertainties and external disturbances, demonstrating good performance.

The rest of the paper is organized as follows: Section 2 introduces our one-degree-aerial device where a PI controller is realized to fulfill the control objective. This controller is instrumented by using analog electronics via operational amplifiers. Besides, our control design includes PWM converters for the generated control signal to the DC motors of the propellers. Stability analysis is also granted. Section 3 shows the experimental results, including a video link of our experiment. First, this section gives a statistical analysis of the PWM signal to its generated control signal to complete the analysis of the performance of the experimental platform. Then, a modification of the experimental platform was done to test its robustness. Finally, Section 4 discusses the results, and Section 5 gives the conclusions of this work.

Notation: $\dot{(\cdot)} = d(\cdot)/dt$ and $\ddot{(\cdot)} = d^2(\cdot)/dt^2$.

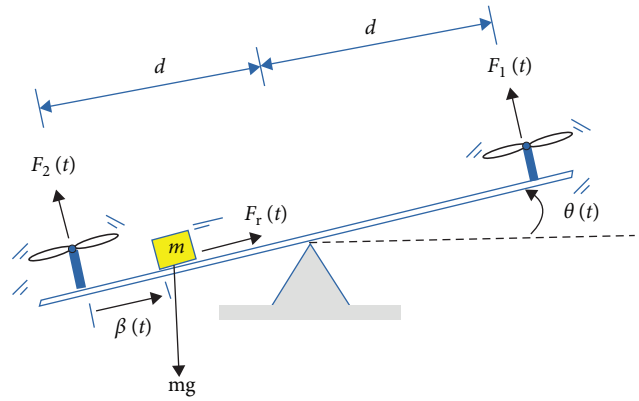

Figure 1: An sketch of the experimental platform. The beam angular position $\theta(t)$ is measured by using a potentiometer, and the mass location $\beta(t)$ is measured by using an optical sensor. The distance d is about 34 cm, and m about 70 g (see Table 1 for notation).

Table 1: Physical specifications.

Notation	Entity
d	Distance propeller-beam center ($d = 34$ cm)
$F_r(t)$	Mass's friction force
$F_1(t)$	Force produced by Propeller 1
$F_2(t)$	Force produced by Propeller 2
m	Cart mass ($m = 70$ g)
$\beta(t)$	Mass position
$\theta(t)$	Beam angular position
g	Gravitation constant ($g = 9.81$ m/s^2)

2. Materials and Methods

The motivation to design an experimental platform emulating an aerial machine arises from the fact that drones, nowadays, have a significant impact on human life [16]. In this respect, we propose the experimental platform shown in Figure 1 (see Table 1 for notation). In Figure 1, we can appreciate two propellers that are driven by DC motors. These are mounted at both ends of a beam. This beam is pivoted at its center.

Additionally, we have a mass placed on the beam. This mass slides on the beam due to gravity and the vibrations induced by the propellers on the beam. Hence, friction force on the mass is a nonlinear effect depending on the beam rotation and structure vibrations, among others. A photo of the experimental platform is shown in Figure 2. This system is open-loop unstable. Our control objective is as follows.

2.1. Control Objective. Given the measurable variables from our experimental platform, $\theta(t)$ and $\beta(t)$, design a controller block such that $F_1(t)$ and $F_2(t)$ produce control action on the aerial device satisfying as follows:

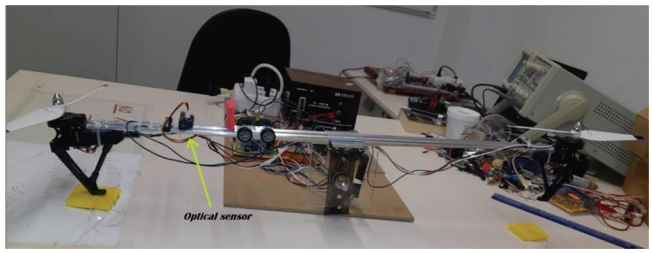

Figure 2: A photo of the experimental platform. A video link of the experimental platform is here. The car's wheels are utilized as barriers to keep the car moving on the beam. Therefore, the car slips on its tummy. Additionally, in front of the car, an optical sensor is fixed. This sensor is to measure $\beta(t)$. Its weight is about 60 g.

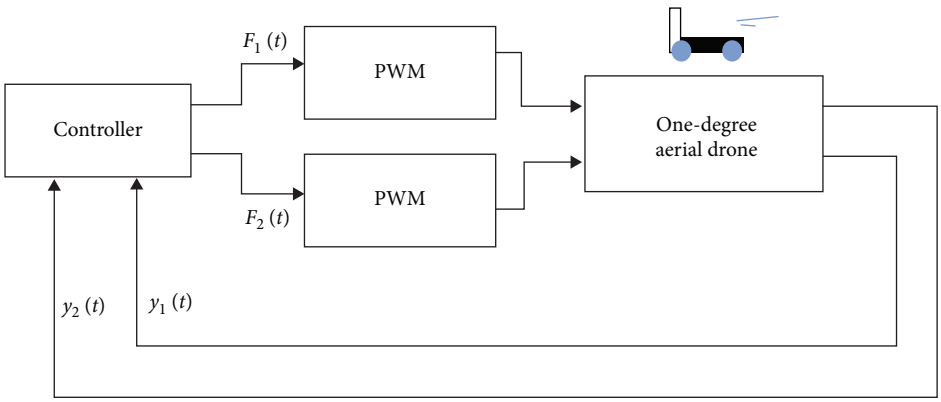

Figure 3: The closed-loop system of the experimental platform. The PWM block converters are shown too. The reference command is given inside the controller block. Here, $y_1(t) = \theta(t)$ and $y_2(t) = \beta(t)$.

$$|\theta(t)| \leq \beta_1, \ |\beta(t)| \leq \beta_2, \tag{1}$$

and

$$|\dot{\theta}(t)| \approx 0, \ |\dot{\beta}(t)| \approx 0. \tag{2}$$

The control objective primarily aims to regulate the positions of both the beam and the moving car, ensuring their proximity to the desired location and achieving near-stationary states. The parameters β_1 and β_2 represent constant upper bounds determined by mechanical and electronic limitations.

2.2. Control Design. The primary goal of this section is to demonstrate our control design, which effectively fulfills the objectives outlined in the preceding section. Our proposed approach involves implementing a PI controller through analog electronics, complemented by the incorporation of corresponding PWM converters in our design. In Figure 3, the closed-loop control scheme is depicted. The first part of our control design is shown in Figure 4. In Figure 4, let us define $u(t)$ as the control signal at point A. Then, the optical sensor obtains the $\beta(t)$ value for the range from 0.5 to 6 cm, giving a value between 0.05 and 3 V, respectively. This distance range, according to the optical sensor manufacturer, is linear. The manufacturer of the optical sensor is the Sharp company (item number GP2Y0A41SKOF).

After conducting a basic circuit analysis using the schematic depicted in Figure 4, we derived the following equation for the control law:

$$\begin{aligned} cu(t) = & \left[\frac{1}{G_a} + \frac{1}{2.2k}\right] G_a \left[-\frac{\theta(t)}{2.2k} - \frac{\beta(t)}{2.2k}\right] \\ & + \left[\left(\frac{1}{G_a} + \frac{1}{2.2k}\right)\left(\frac{G_a + 1.1k}{1.1k}\right) - 1\right] v^- \\ & + cG_a \left[-\frac{d\theta(t)}{dt} - \frac{d\beta(t)}{dt}\right] - \frac{u}{2.2k} \end{aligned} \tag{3}$$

$$v^- = 3.37x10^{-6} w + 1.89x10^{-7} O_s, \tag{4}$$

where $k = 10^3$, $c = 47$ pF is a control gain, and G_a is the controller gain adjusted via a trimmer, as shown in Figure 4. Then, the above control signal $u(t)$ is supplied to the circuit given in Figure 5. In Figure 5, the positive part of $u(t)$ is extracted by the positive half-wave rectifier and the negative one by the negative half-wave rectifier. So, Figure 5 illustrates the electronic circuit designed to separate the negative and positive components of $u(t)$ (3). In this last, a voltage inverter is realized by the operational amplifier. Figure 6 shows the PWM converter using the integrated circuit TL594. This integrated circuit is popular in electronics [17, 18].

Observing the control law stated in Equations (3) and (4), it has the following compact format:

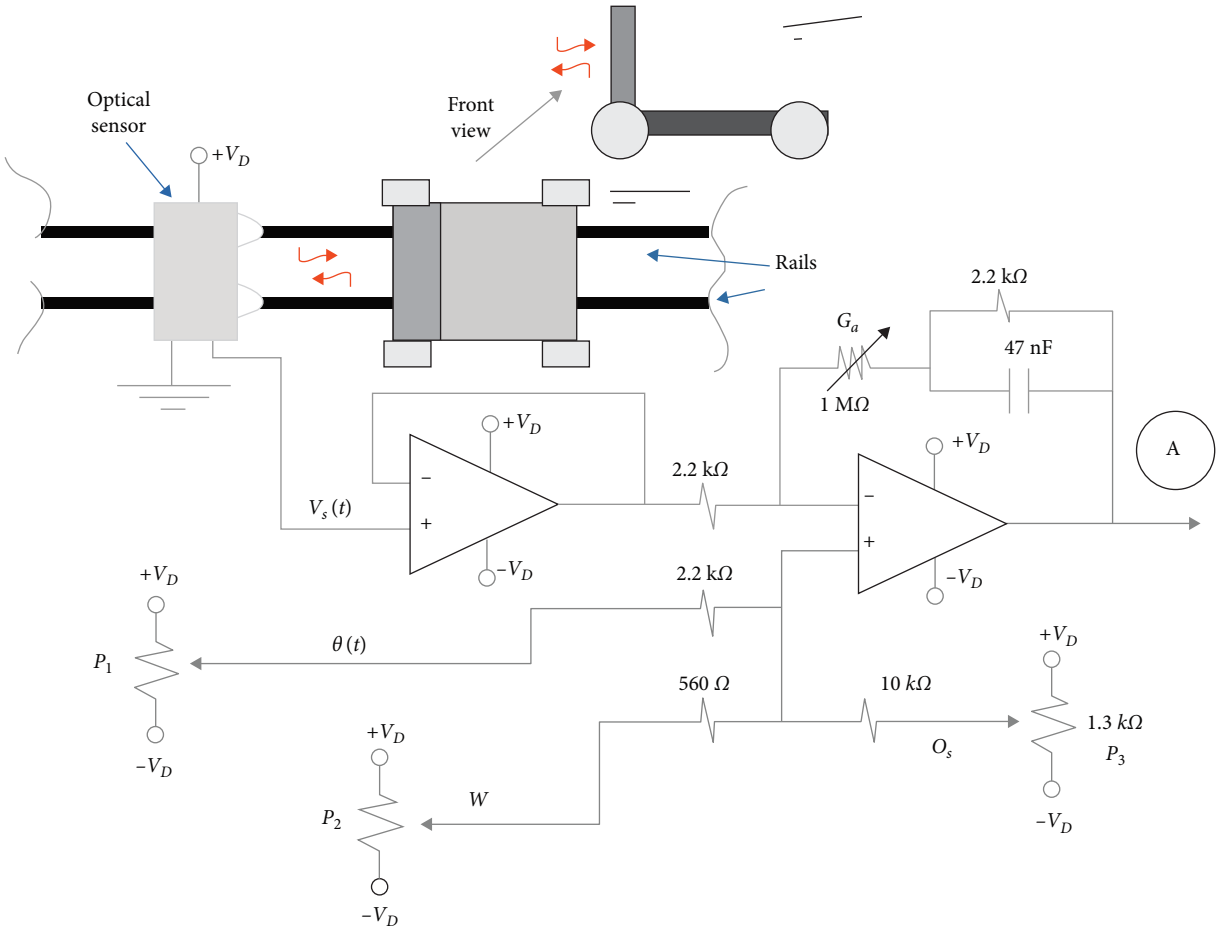

FIGURE 4: Optical sensor instrumentation and control law. $P_1 = 1$ kΩ is the potentiometer to instrument $\theta(t)$. $P_2 = 47$ kΩ and $P_3 = 1.3$ kΩ are potentiometers to tune the control law. G_a is the controller gain adjusted via a trimmer of 1 MΩ. $v_s(t) = \beta(t)$ is the optical sensor response. The output signal at point A is fed to the second part of the controller, as shown in Figure 5. From this schematic, proportional and integration actions are realized on the input signals by the operational amplifiers. Operational amplifiers are realized by using the integrated circuit LM258. Finally, $\pm V_D = \pm 6$V.

$$\alpha \frac{du(t)}{dt} = -k_1\theta(t) - k_2\beta(t) + \rho - k_3\frac{d\theta(t)}{dt} - k_4\frac{d\beta(t)}{dt} - k_5 u(t), \tag{5}$$

where

$$\rho = \left[\left(\frac{1}{G_a} + \frac{1}{2.2k}\right)\left(\frac{G_a + 1.1k}{1.1k}\right) - 1\right]v^{-}. \tag{6}$$

The other parameters can be easily conceived too. Here, ρ is an offset value that is set when the values of G_a, w, and O_s are fixed. Then, the controller structure in Equation (5) is a proportional–integral control.

From experimentation, a set of steps to controller parameters tunning is as follows:

(1) Put potentiometers P_2, P_3, and G_a at their center positions, shown in Figure 4.
(2) Turn on the experiment.
(3) Adjust potentiometer P_2 until the drone propellers are both acting.
(4) Adjust potentiometer P_3 until the system is almost stable and the beam is almost located horizontally.
(5) Finally, adjust the potentiometer G_a to increase the controller performance.

2.3. Stability Analysis of the Closed-Loop System. To analyze the stability of the closed-loop system, we require a simplified plant model of our one-degree-aerial device. From Figure 1, we can obtain the following dynamics model:

$$J\ddot{\theta}(t) = u(t)d - mg\cos(\theta(t))(d - \beta(t)), \tag{7}$$

$$m\ddot{\beta}(t) = mg\sin(\theta(t)) - F_r(\theta(t)), \tag{8}$$

where J and m are the rotational inertia, the car mass, and F_R is the friction on the car body, respectively. It mainly depends on the rotational angle $\theta(t)$, among other factors, of course. Additionally, the above dynamics can be represented as follows:

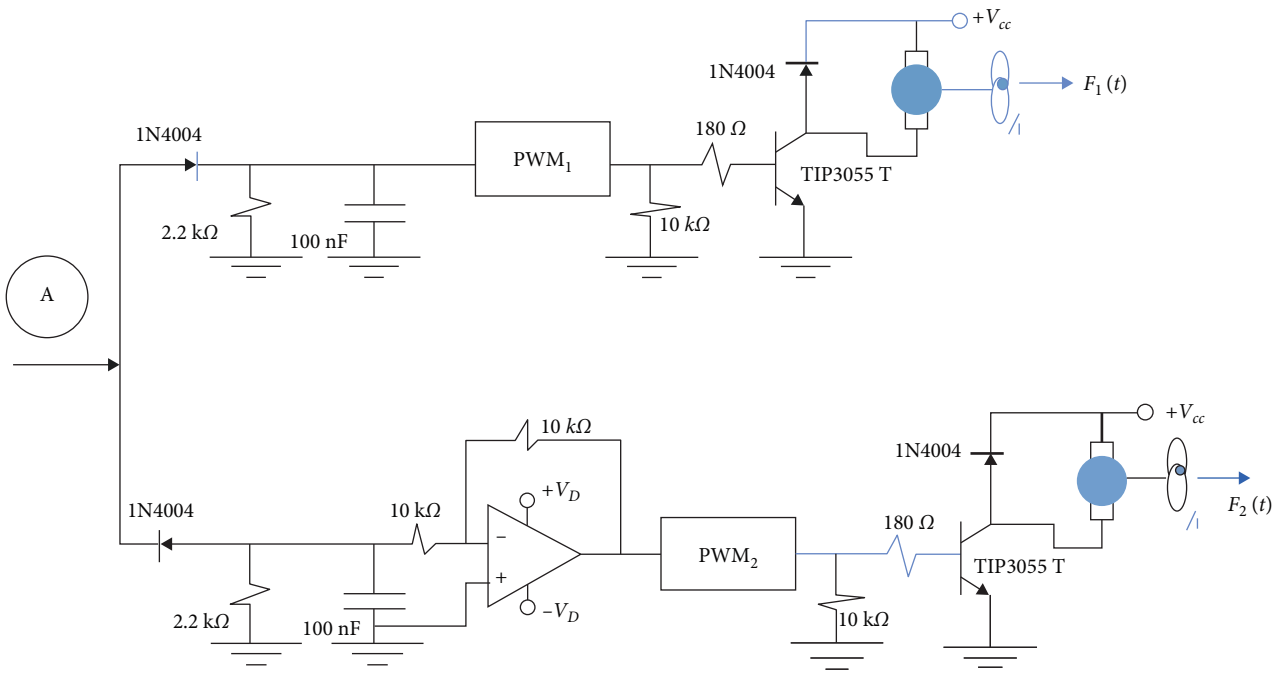

FIGURE 5: Circuit used to separate the control signal $u(t)$ from its positive and negative parts. Each one is converted to a PWM (pulse-width modulation) signal. After that, these are supplied to their respective propeller drivers. Additionally, $v_{cc} = 12\text{V}$. The operational amplifier is realized by using the integrated circuit LM258.

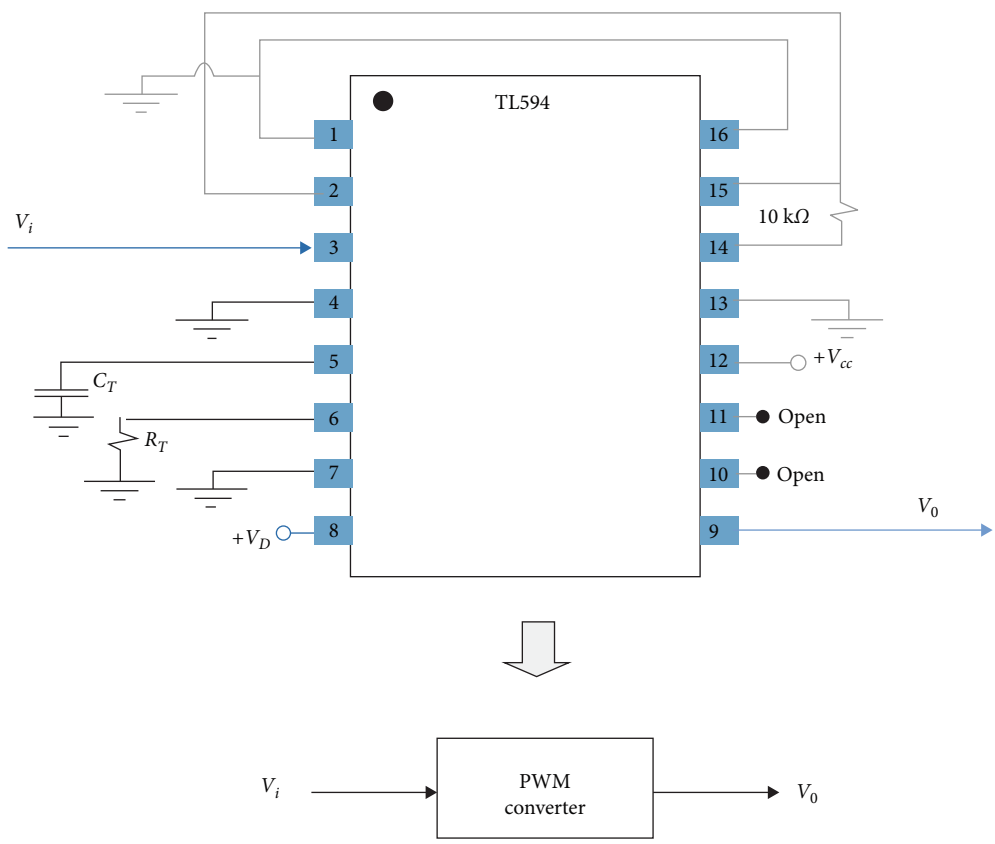

FIGURE 6: Realization of the PWM block by using the integrated circuit TL594. $C_T = 0.001\,\mu\text{F}$ and $R_T = 100\,\text{k}\Omega$ giving a PWM signal frequency $f = 1/R_T C_T = 10\,\text{kHz}$.

$$\frac{d}{dt}\begin{pmatrix}\theta(t)\\ \dot{\theta}(t)\end{pmatrix}=\begin{pmatrix}\dot{\theta}(t)\\ \dfrac{u(t)d}{J}-\dfrac{mg}{J}\cos(\theta(t))(d-\beta(t))\end{pmatrix}, \tag{9}$$

and

$$\frac{d}{dt}\begin{pmatrix}\beta(t)\\ \dot{\beta}(t)\end{pmatrix}=\begin{pmatrix}\dot{\beta}(t)\\ g\sin(\theta(t))-\dfrac{F_r(\theta(t))}{m}\end{pmatrix}. \tag{10}$$

From Equations (9) and (10), and assuming that the friction force $F_r(\theta(t))$ is zero when $\theta(t)=0$, an equilibrium point of the open-loop system occurs if $\theta(t)=\dot{\theta}(t)=\dot{\beta}(t)=0$. So, $\cos(\theta(t))\simeq 1$ and $\sin(\theta(t))\simeq\theta(t)$ in Equations (9) and (10), obtaining a relation between $\beta(t)$ and $u(t)$:

$$\frac{u(t)d}{J}-\frac{mg}{J}(d-\beta(t))=0. \tag{11}$$

From Equation (11), we derived the following:

$$u(t)=\frac{mg(d-\beta(t))}{d}. \tag{12}$$

From the above expression, there exists constant values, u_{ref} and β_{ref}, such that Equation (12) is satisfied with $u(t)=u_{\text{ref}}$ and $\beta(t)=\beta_{\text{ref}}$. Then, using the control law defined in Equation (5), the linear model of the closed-loop system, Equations (9) and (10), is given by the following:

$$\dot{x}(t)=Ax(t)+w_s(t), \tag{13}$$

where

$$x(t)=\left(\theta(t)\ \beta(t)\ \dot{\theta}(t)\ \dot{\beta}(t)\ u(t)\right)^T, \tag{14}$$

$$A=\begin{pmatrix}0 & 0 & 1 & 0 & 0\\ 0 & 0 & 0 & 1 & 0\\ 0 & mg/J & 0 & 0 & d/J\\ g & 0 & 0 & 0 & 0\\ -k_1/\alpha & -k_2/\alpha & -k_3/\alpha & -k_4/\alpha & -k_5/\alpha\end{pmatrix}, \tag{15}$$

and

$$w_s(t)=\begin{pmatrix}0\\ 0\\ 0\\ \dfrac{1}{m}\dfrac{\partial F_r(\theta(t)}{\partial\theta(t)}\Big|_{\theta(t)=0}\\ \rho/\alpha\end{pmatrix}. \tag{16}$$

Note that in Equation (10), the friction term $F_r(\theta(t))$ needs to be linearized using a first-order Taylor series expansion around the operating point. For simplicity, in the above mathematical development, we use $\beta_{\text{ref}}=u_{\text{ref}}=0$, and because the term $F_r(\theta)$ is a nonlinear and unknown term, we use it as a bounded perturbation. Obviously, it is also assumed that J is constant too. To characterize the control parameters in Equation (5), one can utilize the classical roots located in the characteristic polynomial of the linear system in Equation (13). Therefore, for the provided matrix A, Equation (15), its characteristic polynomial is as follows:

$$P(\lambda)=\left(\frac{-k_2dg}{J\alpha}+\frac{mg^2k_5}{\alpha J}\right)-\frac{dgk_4}{J\alpha}\lambda-\frac{dk_1}{J\alpha}\lambda^2-\frac{dk_3}{J\alpha}\lambda^3-\frac{k_5}{\alpha}\lambda^4-\lambda^5. \tag{17}$$

Based on the characteristic polynomial mentioned above, it is evident that the control parameters k_1, k_2, k_3, k_4, and k_5 in Equation (5) have the ability to influence its coefficients. Consequently, these parameters also affect the stability condition of the closed-loop system in Equation (13).

3. Data Experimental Results

This section introduces two experimental setups aimed at demonstrating the performance and robustness of our proposed approach. Initially, a statistical analysis of the PWM signal is conducted to validate the efficacy of the experimental platform. Subsequently, a modified setup is introduced to assess the performance of this novel one-degree aerial device.

3.1. Analysis of PWM Signal. This section shows the experimental results of the controller performance of our one-degree aerial device (another video link: here). The experimental data is given in Figure 7. Because we are using PWM signals in the closed-loop system, to better appreciate the signals in Figure 7, we use a digital low-pass filter given by the following:

$$x[k+1]=x[k]+h(-x[k]+D_s[k]);\ h=0.00667,\ x[0]=0.0, \tag{18}$$

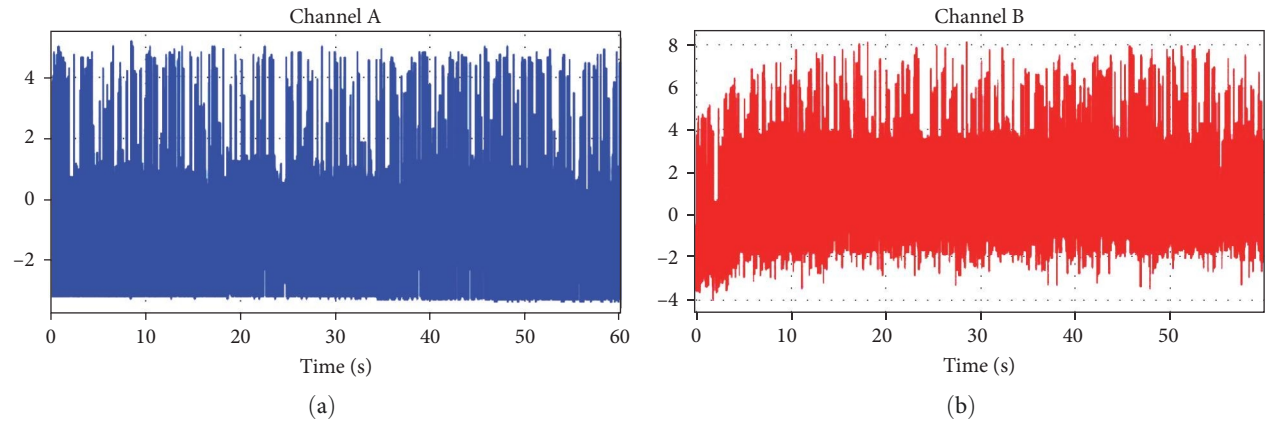

Figure 7: Experimental result. (a) (Channel A): beam angular rotation $\theta(t)$ from the related potentiometer. (b) (Channel B): control signal at point A shown in Figures 4 and 5. Scale vertical axis in volts.

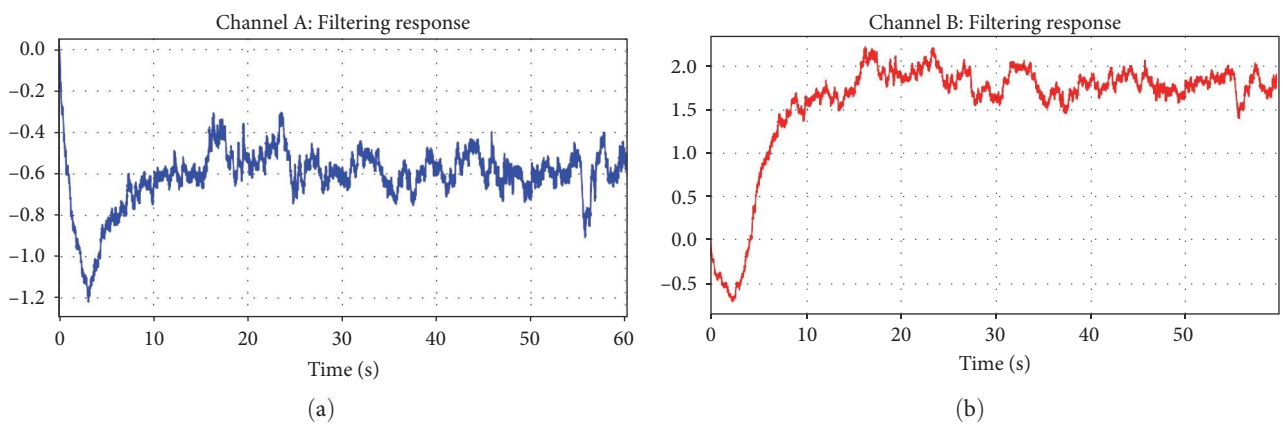

Figure 8: Filtering signals (from Figure 7) to better appreciate the closed-loop control performance. (a) (Channel A): beam angular rotation $\theta(t)$; (b) (Channel B): control signal, with scale vertical axis in volts.

where h, in seconds, is the sampling time of the data capture, k is the data pointer, and $D_s[k]$ is either the data in Channel A or Channel B in Figure 7. Figure 8 shows the related data processing. Just to recall, the motor is itself a low pass filter, among other electronics in our experimental platform. Then, by realizing classical statistical analysis to conclude that the processed data have the same information as the raw signal from the average point of view of the signal, we proceed as follows.

The analysis of variance (ANOVA) technique indicates that there is no significant difference between the mean values of the data for Channel A and the mean values for the filtered angular position beam (Channel A). Likewise, the analysis demonstrates that there is no significant difference between the mean values of the control signal (Channel B) and the mean values for the filtered control signal. In other words, the ANOVA test results suggest that the filtering process applied to the data did not cause any substantial alteration in the mean values of the respective channels. This finding implies that the filtering method used was effective in retaining essential information without significantly affecting the central tendency of the data in both the angular position beam (Channel A) and control signal (Channel B). After conducting experiments, we have observed a remarkable control performance from our experimental platform when employing a PI controller with analog electronics.

The car's position is illustrated in Figure 9. Since the acquisition board possesses only two channels, a subsequent experiment was conducted to capture the mass position $\beta(t)$. To demonstrate the control behavior, an external disturbance was deliberately introduced, showcasing the regulation that steers the car's position towards $\beta_{\text{ref}} = 0$. The cart's position behavior was analyzed using the same digital filter as specified in Equation (18) and applied to the experimental data. The manual cart position perturbations are indicated by the black arrows.

3.2. Experimental Results: Perturbed Case. Although the given experimental platform already presents some kind of perturbation in the dynamic modeling due to the moving mass of the car emulator, another experiment for a perturbed case is presented in this section. In this case, the disturbance consists of adding a disturbing mass to a propeller of the aerial device. Figure 10 displays a photograph of the modified experiment, featuring an additional mass attached to propeller 1. In Figure 10, the disturbance mass weighs 1.3 g and is

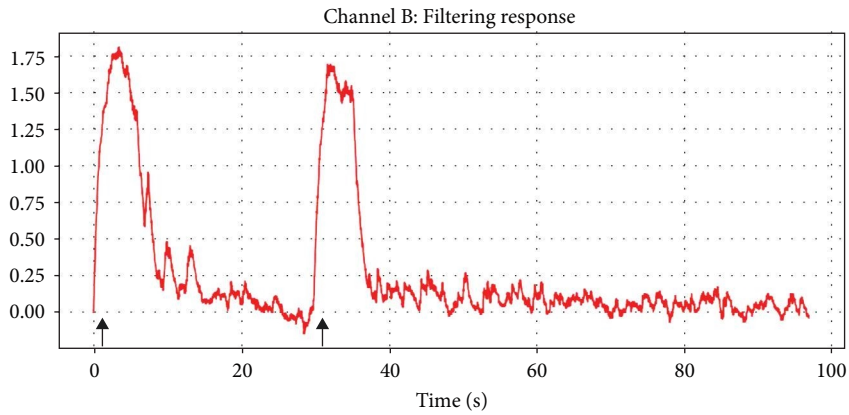

Figure 9: Cart's position behavior, with scale vertical axis in volts. The identical digital filter provided in Equation (18) based on the data obtained from experimentation was used. The black arrows indicate the by-hand cart position perturbations.

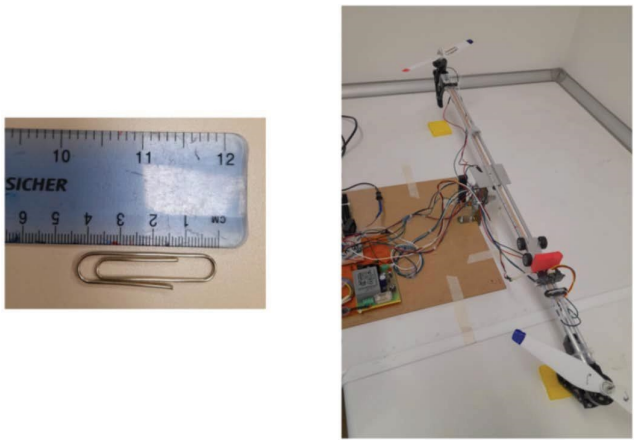

Figure 10: Photo of the modified experiment. The disturbance mass weighs 1.3 g and is approximately 4.5 cm long. Link to the video: here or in YouTube.

approximately 4.5 cm long. This body is attached to the cited propeller by using tape. In addition, we slightly increased the controller gain to visually appreciate the control action of the closed-loop system. See the video link (attached here). Also, to highlight, the added disturbance alters many dynamic characteristics of the aerial device, a strong disturbance for the controller. Based on the data obtained from the perturbed system, the assessment of the controlled system's robustness is established.

4. Discussion

The experimental platform introduced in this paper represents a novel benchmark for conducting control tests. In order to assess its performance, a PI controller has been devised to serve as a performance reference. As far as the authors are aware, there are no existing references or previous works specifically addressing this design. Evaluating the closed-loop robustness typically involves testing how well a control system maintains stability and performance in the face of unexpected changes or uncertainties. One way to assess this is by deliberately introducing disturbances or variations into the system, which could mimic real-world scenarios where the model might not perfectly represent all factors influencing the system. For instance, adding a mass to a propeller could create an unexpected change in the system dynamics, allowing researchers to observe how well the control mechanism adapts to such alterations and maintains desired performance despite these disturbances. Additionally, to highlight, we intentionally increase the controllers' gains to better visualize the control performance of closed-loop dynamics (see video here).

This paper presents an analog instrumentation platform and introduces an analog implementation of a PI controller. However, more advanced controllers, such as SMC or other nonlinear control laws, can be implemented through programing. Implementing a nonlinear controller using analog electronics is not as straightforward as our initial design suggests. For instance, upon sending the acquired data to the computer, a digital controller can be defined and tested. Dealing with real experiments, the time response of the system poses a significant challenge in design. Therefore, the real challenge lies in achieving a desirable time response for the system, typical in experimental setups. The PI control law delineated in this paper serves as a benchmark to evaluate the efficacy of the new strategy. It can be considered a reference point to conclude the viability and effectiveness of the newly proposed approach. Furthermore, the current platform has been instrumental in understanding design limitations and has significantly advanced the knowledge of implementing analog controllers on quadrotors, serving as a focal point for future work.

5. Conclusion

This paper presents a step-by-step construction of a two-rotor device capable of reproducing the ball and beam problem while being subjected to external disturbances and unmodeled dynamics. The mobile object experiences friction and the control strategy drives it to a predefined position. A stability analysis demonstrates that the control objective of boundedness is achieved. Additionally, an ANOVA test indicates that the filtered data retain essential information. The

resulting experimental platform is not only low-cost but also serves as a benchmark for testing various control algorithms. Here, a PI control was designed to solve the regulation problem. This PI controller has proven to be highly effective in achieving our desired control objectives and maintaining system stability. These positive results underscore the practicality and efficiency of the chosen control approach, demonstrating its potential for real-world applications. The successful outcomes obtained through the PI controller validate the significance and value of our experimental platform as a suitable testbed for evaluating and refining control algorithms for aerial machines or similar systems. Moreover, a modification of the experimental setup was introduced to effectively study the robustness of adding a mass on one propeller. This experimentation helps in verifying the system's resilience and its capability to handle unpredictable conditions, providing insights into its robustness and effectiveness.

By creating an experimental platform that replicates the behavior of an aerial machine, researchers and engineers can conduct controlled experiments and tests to develop and refine drone technologies. This can lead to advancements in drone control algorithms, stability analysis, navigation systems, and fault-tolerance mechanisms. Additionally, having a low-cost experimental platform allows for more extensive research and accessibility to a broader community of researchers, accelerating progress in the field.

Abbreviations

PI: Proportional integral
PID: Proportional integral derivative.

Data Availability

No data are available for this study.

Conflicts of Interest

The authors declare that they have no conflicts of interest.

Acknowledgments

This work has been funded by the Generalitat de Catalunya through the research project 2021-SGR-01044.

References

[1] N. H. Jo and J. H. Seo, "A state observer for nonlinear systems and its application to ball and beam system," *IEEE Transactions on Automatic Control*, vol. 45, no. 5, pp. 968–973, 2000.

[2] W. Yu, "Nonlinear PD regulation for ball and beam system," *International Journal of Electrical Engineering & Education*, vol. 46, no. 1, pp. 59–73, 2009.

[3] A. Burghardt and J. Giergiel, "Modelling and control of a underactuated sphere and beam system," *Communications in Nonlinear Science and Numerical Simulation*, vol. 16, no. 5, pp. 2350–2354, 2011.

[4] B. Hamed, "Application of a LabVIEW for real-time control of ball and beam system," *IACSIT-International Journal of Engineering and Technology*, vol. 2, no. 4, pp. 401–407, 2010.

[5] M. Saad and M. Khalallah, "Design and implementation of an embedded ball-beam controller using PID algorithm," *Universal Journal of Control and Automation*, vol. 5, no. 4, pp. 63–70, 2017.

[6] B. Lawrence, "Tuning of a PID controller for optimal performance of ball and beam system," *International Journal of Engineering Research & Technology (IJERT)*, vol. 9, no. 4, pp. 1–5, 2020.

[7] G. Dewantoro, D. Susilo, and D. C. Amanda, "Development of microcontroller-based ball and beam trainer kit," *Indonesian Journal of Electrical Engineering and Informatics (IJEEI)*, vol. 3, no. 1, pp. 45–54, 2015.

[8] I. A. Hashim, E. H. Karam, and N. S. Abdul-Jaleel, "Design and implementation of a two stage controller for ball and beam system using FPGA," *Engineering and Technology Journal*, vol. 36, no. 4A, pp. 381–390, 2018.

[9] I. K. Yousufzai, F. Waheed, Q. Khan, A. I. Bhatti, R. Ullah, and R. Akmeliawati, "A linear parameter varying strategy based integral sliding mode control protocol development and its implementation on ball and beam balancer," *IEEE Access*, vol. 9, pp. 74437–74445, 2021.

[10] T. Sato, Y. Sakai, N. Kawaguchi et al., "Data-driven response estimation-based tuning and its validation using a ball-and-beam system," in *2023 IEEE 28th International Conference on Emerging Technologies and Factory Automation (ETFA)*, pp. 1–7, IEEE, Sinaia, Romania, September 2023.

[11] A. Matus-Vargas, G. Rodriguez-Gomez, and J. Martinez-Carranza, "Ground effect on rotorcraft unmanned aerial vehicles: a review," *Intelligent Service Robotics*, vol. 14, no. 1, pp. 99–118, 2021.

[12] A. N. Vargas, M. A. Montezuma, X. Liu, L. Xu, and X. Yu, "Sliding-mode control for stabilizing high-order stochastic systems: application to one-degree-of-freedom aerial device," *IEEE Transactions on Systems, Man, and Cybernetics: Systems*, vol. 50, no. 11, pp. 4318–4325, 2020.

[13] K. M. Raza, K. Mohd, and P. Kumar, "Speed control of DC motor by using PWM," *International Journal of Advanced Research in Computer and Communication Engineering*, vol. 5, no. 4, pp. 307–309, 2016.

[14] A. S. M. Bakibillah, N. Rahman, and M. A. U. Zaman, "Microcontroller based closed loop speed control of DC motor using PWM technique," *International Journal of Computer Applications*, vol. 108, no. 14, pp. 15–18, 2014.

[15] R. Chai, K. Chen, L. Cui, S. Chai, G. Inalhan, and A. Tsourdos, "Review of advanced trajectory optimization methods," in *Advanced Trajectory Optimization, Guidance and Control Strategies for Aerospace Vehicles*, Springer Aerospace Technology, pp. 3–42, Springer, Singapore, 2023.

[16] H. González-Jorge, J. Martínez-Sánchez, M. Bueno, and P. Arias, "Unmanned aerial systems for civil applications: a review," *Drones*, vol. 1, no. 1, Article ID 2, 2017.

[17] X. Zhou, D. Chen, and C. Jamerson, "Leading-edge modulation voltage-mode control with flux unbalance correction for push-pull converter," in *APEC 2000. Fifteenth Annual IEEE Applied Power Electronics Conference and Exposition (Cat. No.00CH37058)*, pp. 327–333, IEEE, New Orleans, LA, USA, February 2000.

[18] E. Mujjalinvimut, P. N. N. Ayudhya, and A. Sangswang, "An improved asymmetrical half-bridge converter with self-driven synchronous rectifier for dimmable LED lighting," *IEEE Transactions on Industrial Electronics*, vol. 63, no. 2, pp. 913–925, 2016.